

# PHOTOGRAMMETRIC SURVEY OF THE SURF ZONE FOR CALIBRATION AND VALIDATION OF NUMERICAL MODELS

STEFAN SCHIMMELS, WERNER ZIELKE

*Institute of Fluid Mechanics, University of Hannover,  
Appelstr. 9a, 30167 Hannover, Germany*

FOLKE SANTEL, CHRISTIAN HEIPKE

*Institute of Photogrammetry and GeoInformation, University of Hannover,  
Nienburger Str. 1, 30167 Hannover, Germany*

The calibration and validation of highly developed numerical models for the calculation of wave kinematics inside the surf zone is a difficult task. With photogrammetric techniques it is possible to cover a large area and obtain digital water surface models with high resolution in space and time. These surface models are very well suited to provide boundary conditions for a numerical model and can also serve as a reference for the numerical simulation everywhere inside the area of analysis. This paper describes a photogrammetric method developed over the last years for deriving digital surface models from stereoscopic image sequences and compares numerical simulations with a Boussinesq model based on conventional measurements and photogrammetric data.

## 1. Introduction

The numerical simulation of waves and currents has made huge progress during the last decades. Due to the development of new numerical methods and the computational power of modern computers, today we are able to model physical processes with high resolution in space and time.

Every numerical model has to be validated with analytical solutions or measurements in the laboratory or nature. However, almost all measurements suffer from either giving only a high resolution in time at a fixed position or providing time averaged data over a larger spatial area. Particle Image Velocimetry (PIV) may be mentioned as possibly the only exception to these restrictions, but even this technique is still far away from being useful for large scale measurements in the field.

The use of digital photogrammetry can provide water surface models with the required temporal and spatial resolution (Strybny et al. 2001). Digital image matching was already employed successfully for the determination of wave parameters from stereo images in the past, e.g. (Redweik 1993). Further examples for the determination of sea surfaces using stereo images are given in (Holland et al. 1997), (Taguchi and Tsuru 1998) and (Yamazaki et al. 1998).

This paper describes a photogrammetric method developed over the last years for deriving digital surface models from stereoscopic image sequences and compares numerical simulations with a Boussinesq type model based on conventional point measurements and photogrammetric data.

## 2. Database and Measurement Setup

The area under investigation is a 200 by 200 m<sup>2</sup> groyne field at the island Norderney in the German bight (Figure 1). For image acquisition four digital video cameras were used. The CCD-sensor has a radiometric resolution of 10 bit and a geometrical resolution of  $6.7 \times 6.7 \mu\text{m}^2$  per pixel. The frame sensor size is 1296 x 1031 pixel, the maximum frame frequency is 12 frames per second. The system allows for a maximum observation period of 20 minutes. For synchronization of the cameras the exposure time is controlled by an external trigger signal.



Figure 1. Area under investigation.

Image acquisition was carried out from the top of two high buildings close to the groyne field (white dots in Figure 1). On each building two cameras were set up. Due to the altitude of the camera positions of about 40 m and a maximum distance of 400 m at the outer boundary of the area under investigation, the cameras point downwards with an angle of approximately 10 degrees. This camera constellation results in two overlapping stereo models I/II and III/IV (see Figure 2). The analysis of the entire groyne field is achieved by combining the two overlapping stereo models. The orientation of the images was established manually after image acquisition. The orientation parameters are assumed to be constant for the acquisition of an image sequence.

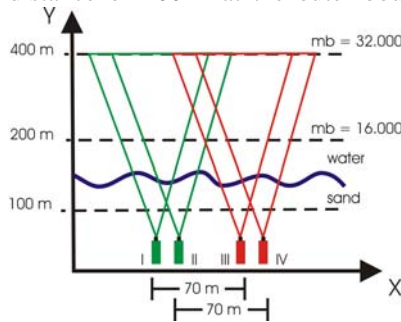


Figure 2. Camera constellation in planimetry.

The center of the area to be investigated has a distance from the cameras of approximately 200 m. At this distance the images have a scale of about 1 : 16 000. Assuming an accuracy of the image coordinates of 1 pixel ( $6.7 \mu\text{m}$ ) in image space, a theoretical standard deviation of 10.7 cm in X and Z, and 119.1 cm in Y is obtained using standard error propagation formulae for one

stereo pair. The poor accuracy in  $Y$  reflects the small stereo base. From the point of view of the application, however, the  $Z$ -accuracy is the most critical one and the reported values satisfy the requirements.

In addition to the photogrammetric image acquisition several conventional measurements were carried out using three waverider buoys, two wave gauges (WD1, WD2), pressure transducers (O1-O3, M1-M3, W1-W2) and a tide gauge. Their positions are shown in Figure 3 over a contour plot of the topography of the groyne field.

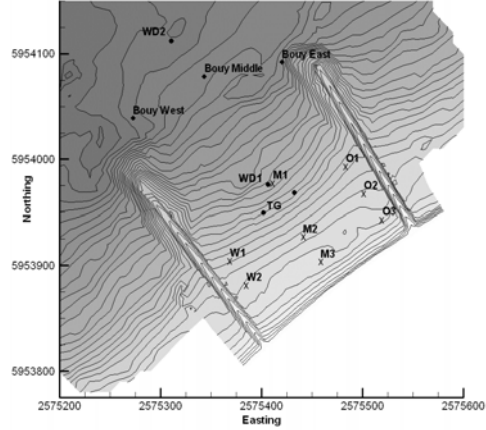


Figure 3. Topography and conventional measurements.

### 3. Numerical Model

To simulate the sea state inside the groyne field a Boussinesq model with a (4,4)-Padé approximation of the linear dispersion relation and a parameterized optimization of the linear shoaling behavior is used (Schröter et al. 1994). The equations are solved on a rectangular grid with a finite difference scheme, which is third order in space and second order in time.

Waves are generated close to the boundary by a mass source which is defined parallel to the boundary and distributed perpendicular to it by a Gaussian shape function (Wei et al. 1999). Discretizing a directional spectrum in  $N$  frequencies and  $M$  directions and generating waves e.g. at the northern end of a computational domain leads to the following source function:

$$f(x, y, t) = \sum_{i=1}^N \sum_{j=1}^M A_{S_{i,j}} \cdot e^{-\beta_i(y-y_s)^2} \cdot \cos(k_i \cos(\theta_j)x - \omega_i t + \varphi_{i,j}) \quad (1)$$

where the exponential term defines the Gaussian shape function and  $A_S$  is the amplitude of the mass source, which is related to the governing equations.

Wave breaking is considered by an eddy viscosity term in the momentum equations, e.g. (Kennedy et al. 2000). The initiation of wave breaking depends on the horizontal particle velocity vector at the free surface  $\mathbf{u}_s$ . Energy dissipation is localized at the front face of the wave requiring the vertical particle velocity at the free surface  $w_s$  to be greater than zero. The breaking criterion can be written as:

$$|\mathbf{u}_s| > \gamma c \quad \text{and} \quad w_s > 0 \quad (2)$$

where  $c$  is the phase velocity in shallow water and  $\gamma$  is a calibration parameter for the initialization of wave breaking, which is typically set to 0.8.

Runup of waves at the beach can easily be simulated with the wet-slope concept (Strybny 2004) where a thin residual water film is assumed at dry nodes. The thickness of the water film  $\varepsilon$  is usually two orders of magnitude less than the grid length and to stabilize the scheme, nodes are set to be dry if the water depth falls below the threshold  $\varphi \cdot \varepsilon$ , where  $\varphi$  is larger than one. With water depth  $D$ , water surface elevation  $\eta$  and velocity vector  $\mathbf{u}$  the wet-slope scheme can be summarized as follows:

$$\text{If } (\eta + D) < \varphi \cdot \varepsilon \quad \begin{cases} \eta = \varepsilon - D \\ \mathbf{u} = \mathbf{0} \end{cases} \quad (3)$$

The numerical implementations of runup and breaking schemes have been verified and calibrated by comparison with analytical solutions and laboratory experiments. The next step will be to validate the model with measurements in the field (see chapter 6). Prior to discussion of this topic, we introduce in the next two chapters the photogrammetric part of our work.

#### 4. Photogrammetric Method

The computation of a digital surface model from images requires the interior and the exterior orientation of the images as well as homologous points. Assuming the orientation to be given after some manual measurements, the identification and the image coordinate measurement of homologous points in two or more overlapping images via image matching over time remains the major task to be solved.

##### 4.1. Point-wise Correlation

The three-dimensional determination of the water surface is accomplished by digital image matching using stereoscopic images as implemented in the software package LISA (Linder 2003). By successive point-wise matching based on cross correlation over the model area through a sophisticated region growing algorithm starting from given seed points (to be collected manually), a three-dimensional point cloud is generated, subsequently a digital surface model (DSM) is obtained by interpolation.

The point-wise matching algorithm runs as follows: Approximate three-dimensional coordinates for the seed point P, the maximum height variation  $\Delta Z$  in object space and the image orientation parameters are needed as input data. A

straight line is then defined through the centre  $H$  of the camera base  $C'C''$  and the seed point  $P$  (see Figure 4). Also the uppermost point  $U$ , which lies  $\Delta Z/2$  above  $P$ , and the lowermost point  $L$ , which lies  $\Delta Z/2$  below  $P$ , lie on this line. Between  $U$  and  $L$  several points are defined in a way that their distance in image space amounts to approximately one pixel.

Using the collinearity equations all these points are then projected into image space yielding several point pairs ( $P', P''$ ). Square windows of a predefined size are set up around each position in the left image. The window in the right image is defined by projecting the four corners of the window in the left image into

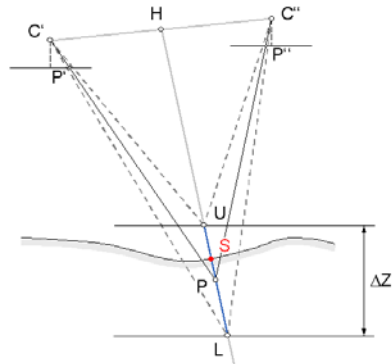


Figure 4. Point-wise matching algorithm.

object space and then into the right image, in both cases using the central perspective transformation. For each pair of windows the cross correlation coefficient  $\rho$  is computed. The window pair with the maximum coefficient  $\rho_{\max}$  is considered to be the pair of conjugate points corresponding to the point  $S$  in object space (see again Figure 4), provided that  $\rho_{\max}$  lies above a pre-specified threshold value. Otherwise the point is rejected.

In order to exclude incorrect correlations, due to small contrast for example,  $\rho_{\max}$  is also checked for uniqueness: From the neighboring five correlation coefficients on either side, the minimum value  $\rho_{\min}$  is selected. If the difference between  $\rho_{\max}$  and  $\rho_{\min}$  is smaller than a value of 0.5, the object point is rejected.

The described principle of point-wise correlation can be considered as a variety of the method of vertical line locus (Bethel 1986). The difference is that points are selected on the line  $HP$  rather than a vertical line through  $P$ .

#### 4.2. Region Growing

A three-dimensional point cloud is generated continuing the point-wise correlation over the entire model area by region growing. Region growing is divided into two parts.

First, the original images are down-sampled. Then, rays in the  $XY$ -plane are defined starting from each seed point into the eight main directions. Using a constant step size in  $X$  and  $Y$  direction, points on these rays are selected. The step size is taken to be equivalent to the grid size of the DSM to be eventually generated. Starting from the results of the seed points, point-wise correlation on the reduced image resolution is carried out for each new point on the rays, al-

ways using the Z value of the previous point as initial height value. Region growing in each direction and for each seed point continues until the correlation fails.

In the next step a regular DSM is interpolated from the resulting three-dimensional points, and point-wise correlation is repeated for each grid node using the original images. Finally, the results are low-pass filtered to eliminate gross errors.

### 4.3. Image Sequence Analysis

The basic idea of processing image sequences in our approach is that in the area of non-breaking waves the change in height of the DSM from one image to the next is very small. This value obviously depends on the recording frequency and must be chosen accordingly. It is then possible to start the process of image matching using only a few manually measured seed points (Santel et al. 2002). Our method is able to find the needed seed points of the following stereo pairs automatically.

In the following the analysis of image sequences is described in more detail (see Figure 5). The matching procedure is executed for the first stereo pair at time step [i]. This leads to a large number of object points. Because of the small wave motion, the object points of the time step [i] can be utilized as seed points for the following time step [i+1]. In order to reduce the matching effort only a pre-specified amount of regularly spaced points generated at step [i] is used as seed points at [i+1]. Matching of the stereo images [i+1] is carried out. Then the results are used in the same way for the stereo images [i+2] and so on.

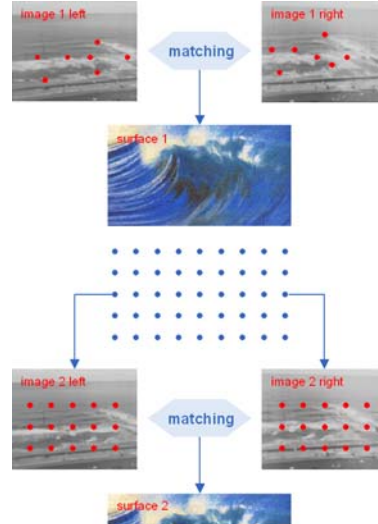


Figure 5. Determination of wave surfaces from image sequences.

## 5. Photogrammetric Results

For the generation of the dynamic DSM approximately 120 well distributed seed points were measured manually in the first stereo pair of an image sequence from cameras III and IV. Using these seed points approximately 60 000 conjugate object points were determined automatically by image matching. Subsequently, matching of a 14½ min image sequence acquired with a frequency of

8 Hz was carried out as described in section 4. The sequence consists of 7 000 images. In the left part of Figure 6 three derived water surfaces of an image sequence with a time difference of 2 s from epoch to epoch are illustrated. The position of the wave peaks can be well identified and tracked in the surface models. Additionally produced orthophotos overlaid to the corresponding surfaces are shown in Figure 6, right. In both illustrations the wave positions coincide. By overlaying the orthophotos the results of image matching are thus visually verified.

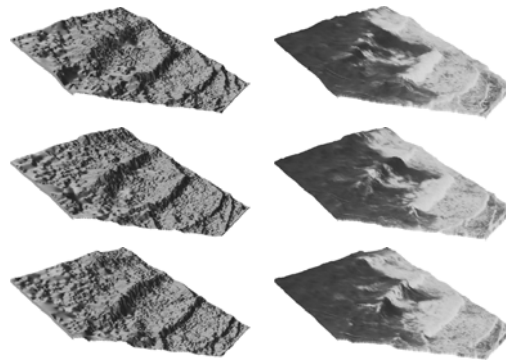


Figure 6. Sequence of water surfaces with  $\Delta t = 2$  s.  
left: surface models; right: overlaid orthophotos

In the following the image matching results are checked by manual analysis and gauge data. The comparison is first carried out with the manual measurement for one epoch and afterwards with the gauge data for multiple epochs.

In the following the image matching results are checked by manual analysis and gauge data. The comparison is first carried out with the manual measurement for one epoch and afterwards with the gauge data for multiple epochs.

### 5.1. One Epoch

The image matching results were spot checked by manual stereo analysis. The manual stereo measurements have been carried out with the Image Station Z IV of Z/I Imaging. For this check the DSM was captured manually twice. The standard deviation in Z derived from double measurements amounts to approximately 10 cm in the surf zone, the results in the seaward area are slightly worse.

The manual measurement was undertaken for several stereo pairs of the image sequence. At each time a part of the entire matched area was analyzed. Figure 7 shows a comparison of image matching and a manual measurement of the entire groyne field with the associated orthophoto.

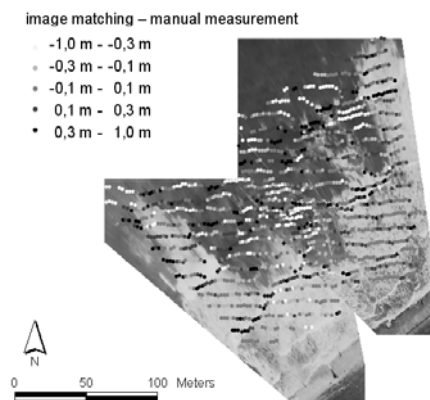


Figure 7. Comparison of image matching and manual measurement with associated orthophoto.

In the manual measurement clearly identifiable points on the sea surface or on the sea spray were captured. The matching algorithm, on the other hand, compares the grey values of the left matching window and the grey values of the corresponding pixels of the right image yielding somewhat different results. In addition errors appear in seaward areas because of the poor texture of the sea surface. The standard deviation between the two surfaces is 29 cm. If the areas with poor texture are disregarded the standard deviation decreases to 21 cm. This corresponds to an accuracy of the image coordinates of 2 pixels.

### 5.2. Multiple Epochs

During the measurement campaign at Norderney Island further measurements with conventional instruments, such as pressure transducers and wave gauges have been carried out. From these point-wise measurements the altitude change of the sea surface can be derived. Using these data the developed photogrammetric procedure was also checked.

Figure 8 represents the image matching results at the position of one of the gauges together with the wave gauge data over a period of 56 s. The 56 s are equal to a sequence of 450 images acquired with a frequency of 8 Hz. The analyzed gauge WD1 is positioned at the centre of the area under investigation (see Figure 3).

As can be seen, the height values determined by image matching correspond to the gauge data very well overall. However, problems arose in the areas of poor texture. Also, some of the peak values of the two curves differ in the range of a few decimeters. It should be noted, that the standard deviation of the gauge data is not known in detail and is estimated to be in the decimeter range.

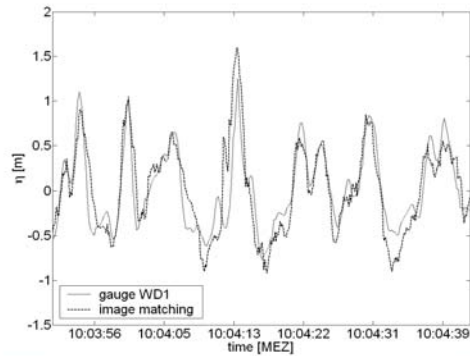


Figure 8. Comparison of image matching results and gauge data WD1.

In order to further analyze the differences between the matching results and the gauge measurements two time steps are compared as examples. These are the times 10:04:09 and 10:04:22. At 10:04:09 the gauge is located in the trough of the wave, and the mismatch occurred due to the poor texture of the sea surface. At 10:04:22 matching is carried out in the turbulent tail of the previous

wave. In this case the difference between the image matching and the gauge data is less than 10 cm, and image matching can be judged to have succeeded.

The standard deviation between the image matching and the wave gauge data was 24 cm. The comparison was also carried out for the pressure transducer M3 located in the surf zone (see Figure 3) with a standard deviation of 10 cm. The difference can be explained by the fact that M3 is located further towards the beach and wave height is less than at position WD1.

## 6. Numerical Simulations

First, the buoy measurements are used to generate waves in the numerical model and the results are compared with the wave gauge and pressure transducers. The disadvantage of this procedure is that we have to make assumptions about the directional spread and the distribution along the boundary for each wave frequency. The waverider buoys provide the horizontal and vertical excursion of the water surface, which can be transformed into mean spectral energy, mean direction and directional spread. Assuming a  $\cos^2$ -distribution in the directional domain we achieve a directional spectrum that can be discretized and applied as wave input for the numerical model using Eq. (1).

Following the above approach we can only reproduce the wave field in a statistical manner, apart from the fact, that we have to make additional assumptions about the directional spread and distribution of waves along the boundary. A comparison of measured data and simulated results is shown in Figure 9 and Figure 10, using data from the middle buoy for wave generation. While the

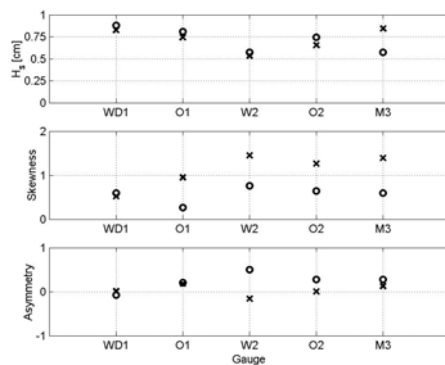


Figure 9. Comparison of statistical parameters.

circles: measurement, crosses: num. simulation

measurements were undertaken, not all instruments have been working properly, so we can only compare the results at five different locations (see Figure 3). Spectral parameters like significant wave height, skewness and asymmetry are shown in Figure 9, while Figure 10 displays energy density spectra at each location. General agreement between measurement data and simulation results is quite good although at some locations there are discrepancies in skewness, asymmetry as well as in spectral energy. Whether these differences result from the numerical model or from wrong assumptions that were put

into the boundary conditions is hard to say. To answer this question it would be helpful to exclude any assumptions about wave directions or distribution along the boundary and furthermore to have more measurements inside the groyne field for comparison.

The photogrammetric results described above can be used to meet these requirements. The principle of using these data for wave generation is illustrated in Figure 11. It shows a DSM for one time step as contour plot together with the boundaries of the computational domain, the shaded source region and the dashed middle line of the source function, where waves are defined.

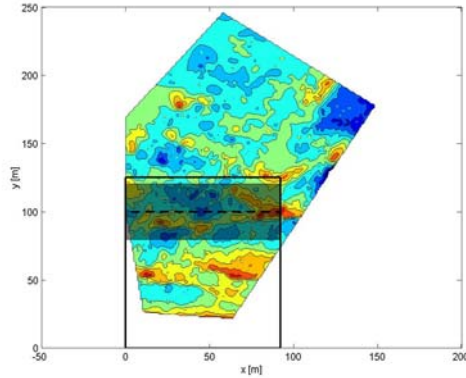


Figure 11. DSM for one time step and computational domain with source function region.

where waves are defined. The data is displayed in a local coordinate system that is parallel to the shoreline and the camera positions. With several DSM at different times we no longer have to make any assumptions about the directional spread and distribution of waves along the boundary. At every node of the source line we get time series of the water surface elevation, which can be transformed into frequency space to give a source function of the form:

$$f(x, t) = \sum_{i=1}^N A_{S_i} \cdot e^{-\beta_i (y - y_s)^2} \cdot \cos(-\omega_i t + \varphi_i) \quad (4)$$

The distribution of waves along the boundary therefore comes directly out of the measured data and wave direction is a result of that distribution.

The weakness of the photogrammetric method is the increasing uncertainty of the measurements with increasing distance from the camera positions and the errors arising in areas with poor texture. For the present case this means, at the

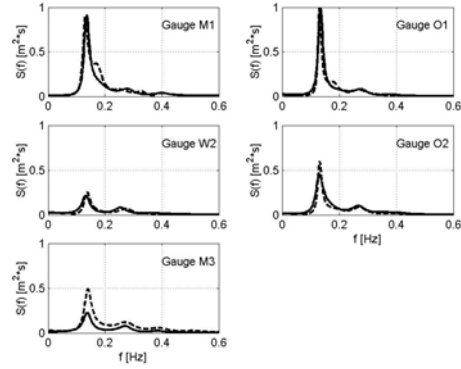


Figure 10. Comparison of energy density spectra.  
solid: measurement, dashed: num. simulation

At every node of the source line we get time series of the water surface elevation, which can be transformed into frequency space to give a source function of the form:

seaward end, where waves are generated, the accuracy of the measurements is worst. For that reason the position of the source function was set to  $y = 100$  m, although there is data available further away. So close to the shoreline waves are already strongly transformed and some of them begin to break. The generation of waves in this area implies further inaccuracies, which should be recognized when interpreting the results below.

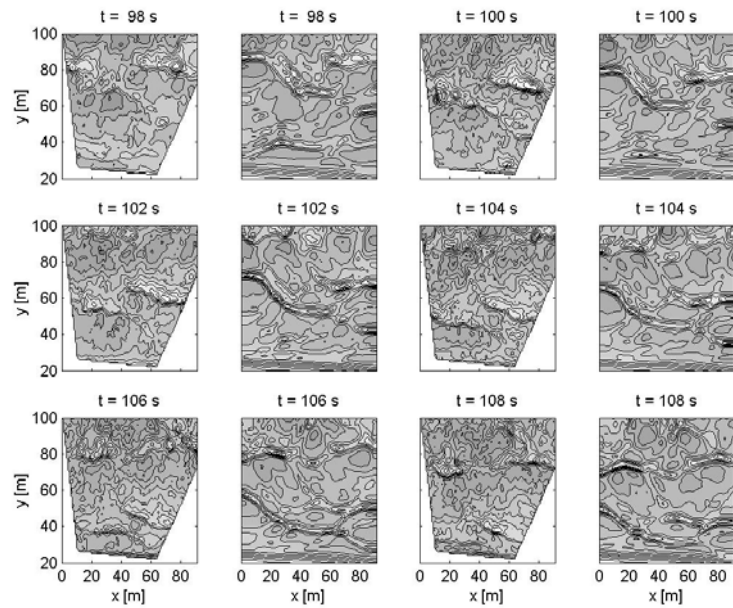


Figure 12. Comparison of spatial water surface elevation at different time steps.  
left image: measurement, right image: num. simulation

Spatial water surface elevations at different times are compared in Figure 12. Although there is no absolute agreement between the measurements in the left images and the simulation in the right, it is evident that the height and direction of the different waves are quite well simulated. This is acknowledged by the time series and energy density spectra at four different locations along the  $y$ -axis for  $x = 40$  m. In principle the data could have been compared everywhere inside the domain and the presented locations are chosen arbitrarily to demonstrate the cross shore evolution of the waves.

Despite the unfavorable location of wave generation and the fact that plunging breaking waves occur in the measurements, differences between measurement and model data are fairly small, in time as well as frequency domain. This gives rise to the assumption, that the numerical model is very well able to simulate the processes inside the surf zone. Hence the dissimilarities of numerical results and point measurements were due to the assumptions in the boundary

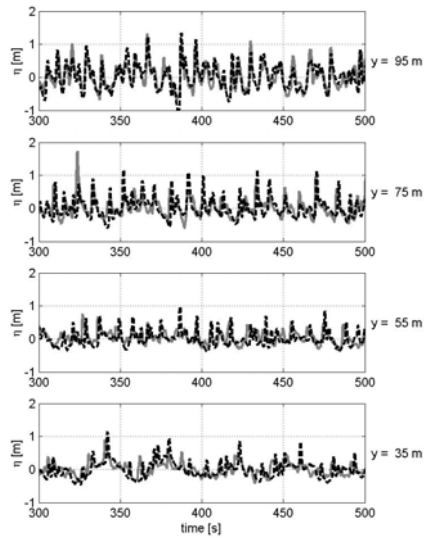


Figure 13. Timeseries of water surface elevation at different locations, ( $x = 40$  m).  
solid: meas., dashed: num. simulation

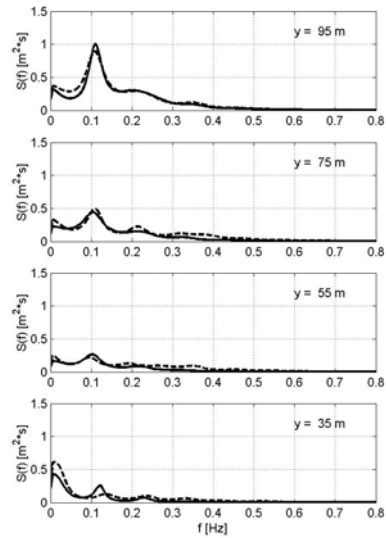


Figure 14. Energy density spectra at different locations ( $x = 40$  m).  
solid: meas., dashed: num. simulation

conditions. In order to prove this assumption, more detailed investigations are necessary, but it can be safely stated that photogrammetry is a valuable tool for this task, even more so if the accuracy of the 3D coordinates is further improved by optimized measurement setups.

## 7. Conclusions

Photogrammetry provides digital water surface models inside a groyne field in time. For the calibration and validation of numerical models these data have two major advantages over conventional point measurements. First, they provide time series of the water surface elevation along the whole boundary, and second, a comparison between measurement and simulation can be made everywhere inside the analyzed domain. However, for a more detailed analysis than the one presented in this paper, it is necessary to optimize the measurement setup. This will further enhance the accuracy of the method and make it a valuable tool for the studying of waves.

## Acknowledgments

The authors are grateful to the Federal Ministry of Education and Research (BMBF) and the German Coastal Engineering Research Council (KFKI) for

funding under the project contract no. 03KIS026, and also for the advice and support received from the Lower Saxony Water Management and Coastal Defense Agency (NLWK) Norden and from the Coastal Research Center (FSK) Norderney of the Lower Saxony State Office for Ecology (NLÖ).

## References

- Bethel, J. 1986. The DSR11 Image Correlator. American Congress on Surveying and Mapping, American Society of Photogrammetry and Remote Sensing. Annual Convention, Vol. IV, 44-49.
- Holland, T., R.A. Holman, T.C. Lippmann and J. Stanley. 1997. Practical Use of Video Imagery in Nearshore Oceanographic Field Studies. *IEEE Journal of Oceanic Engineering*, 22(1), 81-92.
- Kennedy, A.B., Q. Chen, J.T. Kirby, R.A. Dalrymple. 2000. Boussinesq modeling of wave transformation, breaking and runup. Part I: 1D. *Journal of Waterway Port Coastal and Ocean Engineering* 126 (1), 39-47.
- Linder, W. 2003. *Digital Photogrammetry – Theory and Applications*. Springer-Verlag Berlin Heidelberg New York.
- Redweik, G. 1993. Untersuchungen zur Eignung der digitalen Bildzuordnung für die Ableitung von Seegangparametern. *Wissenschaftliche Arbeiten der Fachrichtung Vermessungswesen der Universität Hannover*, Nr. 194.
- Santel, F., C. Heipke, S. Könnecke and H. Wegmann. 2002. Image Sequence Matching for the Determination of three-dimensional Wave Surfaces, *International Archives of Photogrammetry, Remote Sensing and Spatial Information Sciences*, Vol. XXXIV, Part 5, 596-600.
- Strybny, J. 2004. Ein phasenauflösendes Seegangmodell zur Ermittlung von Bemessungsparametern für Küstenstrukturen. *Dissertation, Institute of Fluid Mechanics, Report 69*, in German.
- Strybny, J., H. Wegmann and F. Santel. 2001. Combining Phase-Resolving Wave Models with Photogrammetric Measurement Techniques. *Ocean Wave Measurement and Analysis*, ASCE, Vol. I, 191-200.
- Taguchi, T. and K. Tsuru. 1998. Analysis of Flood by Stereomatching Method. *International Archives of Photogrammetry and Remote Sensing*, Vol. XXXII, Part 5, 810-813.
- Wei, G., J.T. Kirby and A. Sinha. 1999. Generation of waves in Boussinesq models using a source function model. *Coastal Engineering* 36, 271-299.
- Yamazaki, F., M. Hatamoto and M. Kondo. 1998. Utilization of Synchronous Shutter Apparatus in the Photographic Measurement Method of Flood Flow Surfaces. *International Archives of Photogrammetry and Remote Sensing*, Vol. XXXII, Part 5, 848-855.

**KEYWORDS – ICCE 2004**

**Title:**

**PHOTOGRAMMETRIC SURVEY OF THE SURF ZONE FOR  
CALIBRATION AND VALIDATION OF NUMERICAL MODELS**

**Authors:**

Stefan Schimmels, Folke Santel, Werner Zielke, Christian Heipke

**Abstract number:**

338

**Keywords:**

Boussinesq model

Image matching

Photogrammetry

Surf zone

Validation

Video sequences

Wave breaking

Wave runup